2021 43rd Annual International Conference of the
IEEE Engineering in Medicine & Biology Society (EMBC)
Oct 31 - Nov 4, 2021. Virtual Conference

A pipeline for phase-based analysis of *in vitro* micro-electrode array recordings of gastrointestinal slow waves

Julia Y.H. Liu[1], John A. Rudd[1], Peng Du[2]

Abstract — **Motility of the gastrointestinal tract (GI) is governed by an bioelectrical event termed slow waves. Accurately measuring the characteristics of GI slow waves is critical to understanding its role in clinical applications. High-resolution (HR) bioelectrical mapping involves placing a spatially dense array of electrodes directly over the surface of the GI wall to record the spatiotemporal changes in slow waves. A micro-electrode array (MEA) with spatial resolution of 200 µm in an 8x8 configuration was employed to record intestinal slow waves using isolated tissues from small animals including rodents, shrews and ferrets. A filtering, processing, and analytic pipeline was developed to extract useful metrics from the recordings. The pipeline relied on CWT and Hilbert Transform to identify the frequency and phase of the signals, from which the individual activation times of slow waves were identified and clustered using k-means. A structural similarity index was applied to group the major activation patterns. Overall, the pipeline identified 91 cycles of slow waves from 300 s of recordings in mice, with an average frequency of 20.68 ± 0.71 cpm, amplitude of 7.94 ± 2.15 µV, and velocity of 3.64 ± 1.75 mm s^{-1}. Three major propagation patterns were identified during this period. The findings of this study will inform the development of a high throughput software platform for future *in vitro* pharmacological studies using the MEA.**

Clinical Relevance — **The proposed analysis pipeline will be used to quantify response of GI tissues to pharmacological agents.**

I. Introduction

Motility of the gastrointestinal (GI) tract is governed by a bioelectrical activity termed slow waves [1]. In the healthy stomach, gastric slow waves emerge from a pacemaker region in the proximal stomach, and form consecutive bands of propagating wavefronts towards the pylorus [2]. Slow waves emerge from multiple pacemaker sites in the intestine and occur at a higher frequency than gastric slow waves [3]. Both gastric and intestinal slow wave dysrhythmias have been attributed to functional digestive diseases [4], particularly in diabetes [5].

High-resolution (HR) mapping involves placing a spatially-dense 2D array of electrodes on the serosal surface of the GI tract [6]. Using this technique, accurate spatiotemporal characteristics of slow wave propagation can be reconstructed. Traditional HR mapping arrays were manufactured using Ag/AgCl leads embedded in hardened epoxy [6]. More recently, flexible printed circuit (FPC) electrode arrays were manufactured with Au electrodes printed on polyamide substrate [7]. The FPC electrodes are mass producible and easy to sterilize for single or repeated applications in human intra-operative studies [8].

While the FPC electrodes have been deployed to record GI slow waves *in vivo*, an *in vitro* platform with the ability to control the environment is still required for detailed investigations of pharmacological interventions [9], [10]. The inter-electrode spacing of the micro-electrode array (MEA) used for *in vitro* studies is also much finer than the FPC array (0.2 vs 4 mm), which provides a better resolution of the local tissue activation than the standard *in vivo* studies. However, it currently lacks an efficient pipeline for analysis of MEA recordings of GI slow waves. In contrast, *in vivo* HR mapping has established filter settings, activation sequence reconstruction and metrics for analysis [11].

Due to the morphology of the recorded signals with a less pronounced up/down stroke gradient, and the fine inter-electrode spacing, the conventional analysis of AT marking and clustering, followed by manual review may be prone to human error [11], the main objective of this study was to develop an efficient pipeline for the analysis of MEA data in order to inform future high throughput pharmacological studies of the GI system.

II. Methods

A. Experimental Recording

Ethics approval was granted by the Chinese University of Hong Kong Animal Experimentation Ethics Committee. More than 100 datasets from two-month old outbred ICR mice (male, weight 20–25g) were euthanized by carbon dioxide asphyxiation. The whole GI tract was isolated and placed into Krebs' medium gassed with 95 % O_2/ 5 % CO_2. A 10 mm segment of intestine was incubated in Krebs' medium containing nifedipine (1 µM) for 15 min to inhibit movements. Individual segments were mounted on the recording platform of an MEA60 chip (Ayanda Biosystems S.A.) with an 8x8 configuration, with 30-µm 3-D tip-shaped electrodes spaced at intervals of 200 µm. An aluminum brain slice anchor (ALA Scientific Instruments) was placed on top of the tissue to maintain contact. The MEA chip was placed into the recording platform (MEA1060 1200x, Multichannel Systems, Germany) with software-controlled temperature maintained at 35 °C throughout all recordings. Slow waves were sampled at 1 kHz with a calibrated noise density of 15 nV/√Hz using the MC Rack software (v4.6.2, Multichannel Systems). The following sections (B-E) outline the signal processing

This work was funded by a Rutherford Discovery Fellowship from the Rutherford Foundation Trust, Catalyst Grant, and Prime Minister's Emerging Scientist Prize administered by the Royal Society Te Apārangi.

1. J. Y.H. Liu and J. A. Rudd are with School of Biomedical Sciences, Faculty of Medicine, The Chinese University of Hong Kong, Shatin, New Territories, Hong Kong SAR, P.R. China

2. P Du is with the Auckland Bioengineering Institute and Department of Engineering Science, The University of Auckland, New Zealand. Email: peng.du@auckland.ac.nz

pipeline. Signal processing and analysis were performed in MATLAB (R2018b, MathWorks).

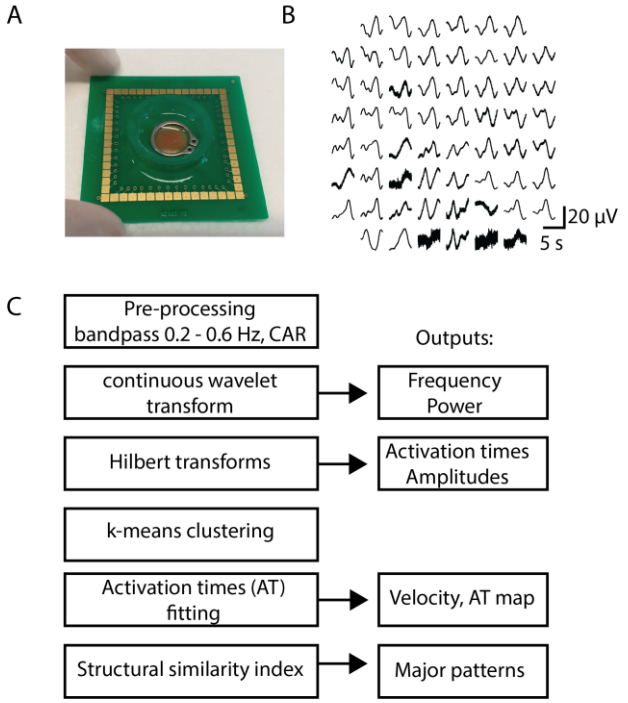

Fig 1. Experimental setup and signal processing outline of MEA recordings of GI slow waves. (A) A photo of the placement of a segment of the intestine mounted on the MEA. (B) Sample raw recordings over a 5 s period. (C) A flowchart showing the general processing steps and the major outputs.

B. *Pre-processing*

The raw signals were filtered with a second order Butterworth filter with a bandpass of 0.2 to 0.8 Hz (12 – 60 cycles per minute (cpm)) and stopband of 0.1 Hz on either side of the pass band with an attenuation of 10 dB. The Butterworth filter was chosen based on its flat bandpass and phase response compared to Chebyshev or elliptic filters which have steep roll-off but ripples in and around the pass bands. A zero-phase filtering scheme was adopted to preserve the phase of the filtered signal. A common average reference (CAR) was subtracted from all the filtered signals. To reduce artifacts induced by interventions, e.g., administering drugs, a 20 s window of data around peaks that were greater than 2 mV was set to 0 μV.

C. *CWT frequency identification*

A continuous wavelet transform (CWT) using a Morse wavelet was applied to the filtered signals, S(t), to identify the change in frequency over time, rather than relying on fixed shifting window of FFT. A CWT filter bank was created based on the CAR containing 83 bands of signals from 0 to 1 Hz. The coefficients of the CWT were averaged across all the channels at each instance in time, and then normalized against the range of the coefficients over the window of analysis. The frequency of slow waves was identified at the frequency that corresponds to the maximum power at each instance in time. Frequencies that were associated with powers that are less than 2 standard deviations of the mean of the power at each instance were eliminated from the analysis. A rolling average filter was then applied to the frequency and power over time. The frequency metric was compared to FFT using a paired Student's t-test by averaging the CWT frequency every 20 s.

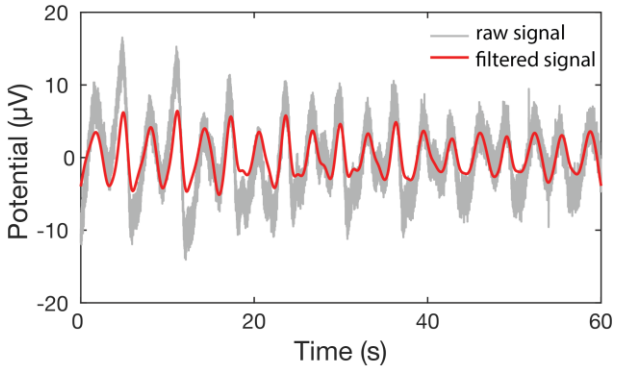

Fig 2. A 60 s sample raw signal trace (light gray) from a single channel on the MEA. The filtered signal is highlighted in red. Over this segment of recording, the frequency was approximately 19 cycles per minute (cpm).

D. *Hilbert Transform*

Given the oscillatory form of the signals around 0 mV, Hilbert transform was applied to S(t) from each channel, from which the instantaneous phase ($\theta(t)$) was calculated using the following expression,

$$\theta(t) = tan^{-1}\left[\frac{imag(HT(S(t))}{real(HT(S(t))}\right] \quad (1)$$

where HT represents the Hilbert transform operator. The activation time (AT) was defined as when the instance phase is equal to 0.5π radians in the phase plot. The amplitude of each detected slow wave was determined as the difference in the recorded potential at ± 50 ms centered around an AT.

E. *Clustering and Analysis*

K-means clustering was applied to the detected ATs every 20 s of the time segment. The number of clusters was determined from the mode of the interval from the CWT analysis. The electrograms were visualized along the y and x directions of the MEA array, with ATs labeled and a line-of-best-fit fitted to each cluster of slow waves in order to indicate the direction of propagation in that particular orientation.

Once all the ATs were clustered, the ATs that were more than 500 ms from the median of each cluster were removed. The remaining ATs were then fitted to a 2D quadratic AT field [12],

$$T(x,y) = ax^2 + by^2 + cx + dy + exy + f \quad (2)$$

where the x and y varied from 0 to 1.4 mm at 0.2 mm increments to match the locations of the electrodes in the MEA. From T(x,y) the velocity field was calculated using the following formula,

$$\begin{bmatrix}\frac{dx}{dt}\\ \frac{dy}{dt}\end{bmatrix} = \begin{bmatrix}\frac{T_x}{T_x^2+T_y^2}\\ \frac{T_y}{T_x^2+T_y^2}\end{bmatrix} \quad (3)$$

where $T_x = \partial T/\partial x$, and $T_y = \partial T/\partial y$. A structural similarity index was computed for each AT map after the offset was subtracted and the remaining times were normalized, using the following expression,

$$SSIM = \frac{(2\mu_1\mu_2+C_1)(2\sigma_{12}+C_2)}{(\mu_1^2+\mu_2^2+C_1)(\sigma_1^2+\sigma_2^2+C_2)} \quad (4)$$

where μ, σ , are the mean, standard devation cross-covariance of T(x,y), and σ_{12} is the cross-covariance between two cycles of T(x,y). Values of C_1 and C_2 were defined from the maximum difference of T(x,y) [13]. The major activation sequences were mapped in a color-coded 2D AT map [11]. The top three most common groups were presented.

III. Results

Stable intestinal slow waves were captured by the MEA over a 300 s period. A total of 91 cycles of gastric slow waves were analyzed, with an average amplitude of 7.94 ± 2.15 µV, and velocity of 3.64 ± 1.75 mm s^{-1}. CWT accurately detected the variations in frequency over time, as shown in Fig. 3. When compared to a standard FFT with a 20 s window, the CWT and FFT produced consistent results (20.68 ± 0.71 vs 20.62 ± 0.83; p-value = 0.43).

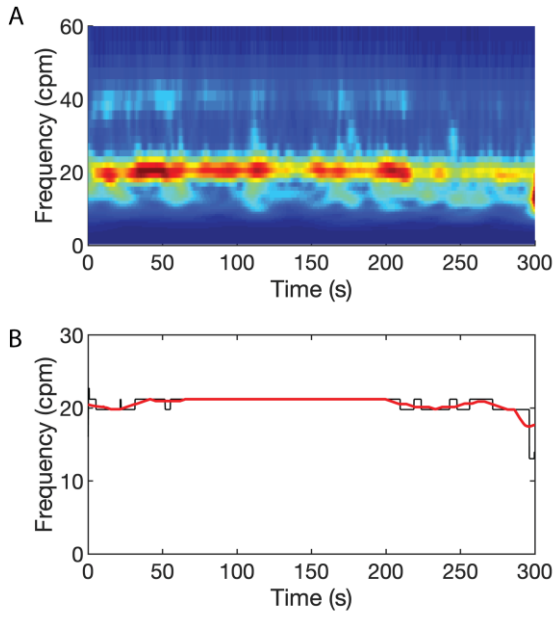

Fig 3. CWT analysis of slow wave frequency. (A) CWT of averaged coefficients at each time instance over 300 s of recording. (B) The dominant frequency at each time instance (black) and its rolling average (red).

The HT also detected the ATs of slow wave throughout the recording, as shown in Fig. 4. When visualized as stacked electrograms, the downstroke of the signals were identified. Following clustering, each cycle of slow wave were partitioned separately and presented as individual AT maps (Fig. 4B), and verified manually by an expert. Over the period known, there appeared to be changes in the propagation direction of slow waves within the MEA. During cycles 4-7 (labeled as small numbers at the bottom of the electrograms in Fig. 4A), slow waves propagated towards the middle of the array, while in the remaining cycles slow waves emerged largely from one corner of the array.

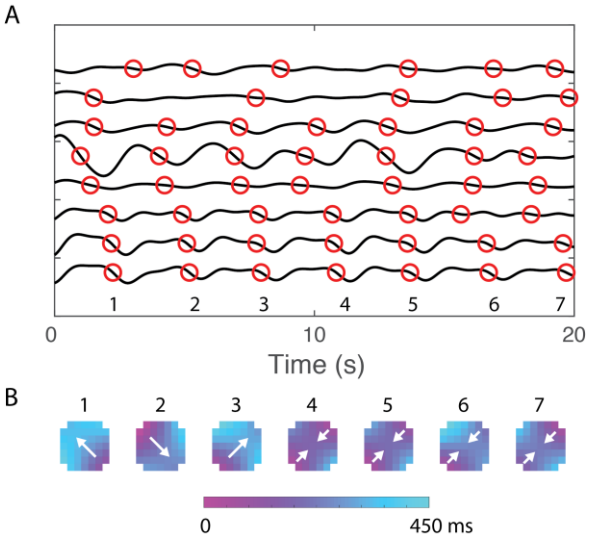

Fig 4. HT detected ATs over a 20 s segment of data. (A) Electrograms from a horizontal row of eight electrodes were selected in the middle of the MEA. The red dots indicate the automatically detected ATs. (B) The reconstructed AT maps over the seven cycles labeled in (A). The white arrows indicate the general direction of propagation.

The SSIM identified three major groups of propagation patterns during the recording, shown in Fig. 5. Together the three groups accounted for 83/91 or over 91% of the total number of cycles identified.

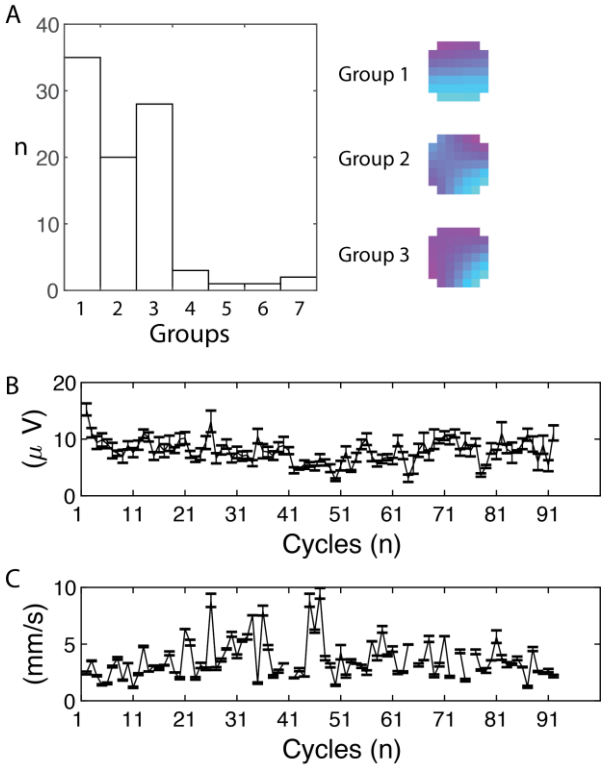

Fig 5. Summary data of the MEA recording. (A) Histogram of the most common groups of propagation patterns defined by the SSIM, with the top 3 groups shown on the right. (B) Amplitude variations over time (91 cycles). (C) Velocity variations over time (3 data points were removed from analysis due to outlier values >10 mm/s).

The most common propagation group occurred in a uniform direction from the top of the MEA (group 1, n = 35). Propagation from the left top corner was the second most common group (group 3, n = 28), and propagation towards the middle of the MEA was the third most common group (group 2, n =20). The transient changes in both amplitude and velocity were also captured, as shown in Fig. 5B and C, respectively. In general, the amplitude was relatively constant throughout the recording, whereas the velocity demonstrated fluctuations near cycle number 25, 35 and 45 (Fig. 5C). The variations in velocity could be due to the instability in the underlying entrainment of GI pacemaker cells [14], and/or from changes in the directionality of propagation [15].

IV. Discussion

A pipeline for filtering, analyzing and visualizing the MEA recordings of GI slow waves was proposed in this study. The initial results demonstrated feasibility in terms of the pipeline to capture the temporal changes of slow waves and classify patterns of propagation.

The MEA represents a significant improvement in the spatial resolution of slow wave in multi-channel HR mapping studies [9]. The controlled *in vitro* environment will also allow precise control of temperatures and delivery of drugs to uncover the mechanisms of specific signaling pathways in the GI tissue [10]. Aspects such as spikes [16], which require much higher sampling rate than slow waves, will also be recorded and anlayzed efficiently using the MEA at 1kHz sampling frequency. However, since k-means is an unsupervised technique, comprehensive validation against groundtruth will be performed in future.

The current configuration of the MEA is a planar 2D system, so analysis is limited to detecting slow waves from the surface only. With the introduction of 3D conducting polymer electrodes it is possible to create protruding arrays to generate better adhesion to the tissue and gather recordings from the transmural direction of the GI wall [17].

V. Conclusions

Activation sequences of GI slow waves were detected at 0.2 mm spatial resolution over 60 electrodes in a MEA at 1 kHz. Further improvements will include more artifact rejection and more efficient performance for high throughput analysis of pharmacological studies.

References

[1] J. D. Huizinga and W. J. Lammers, "Gut peristalsis is governed by a multitude of cooperating mechanisms," *Am. J. Physiol. Gastrointest. Liver Physiol.*, vol. 296, no. 1, pp. G1-8, 2009, doi: 10.1152/ajpgi.90380.2008.

[2] G. O'Grady, P. Du, L. K. Cheng, J. U. Egbuji, W. J. E. P. Lammers, J. A. Windsor, and A. J. Pullan, "Origin and propagation of human gastric slow-wave activity defined by high-resolution mapping.," *Am. J. Physiol. Liver Physiol.*, vol. 299, no. 3, pp. G585–G592, Sep. 2010, doi: 10.1152/ajpgi.00125.2010.

[3] W. J. E. P. Lammers, "Normal and abnormal electrical propagation in the small intestine.," *Acta Physiol. (Oxf).*, vol. 213, no. 2, pp. 349–59, Feb. 2015, doi: 10.1111/apha.12371.

[4] D. A. Carson, G. O'Grady, P. Du, A. A. Gharibans, and C. N. Andrews, "Body surface mapping of the stomach: New directions for clinically evaluating gastric electrical activity.," *Neurogastroenterol. Motil.*, p. e14048, Dec. 2020, doi: 10.1111/nmo.14048.

[5] W. J. Lammers, H. M. Al-Bloushi, S. A. Al-Eisaei, F. A. Al-Dhaheri, B. Stephen, R. John, S. Dhanasekaran, and S. M. Karam, "Slow wave propagation and plasticity of interstitial cells of Cajal in the small intestine of diabetic rats," *Exp. Physiol.*, vol. 96, no. 10, pp. 1039–1048, 2011, doi: 10.1113/expphysiol.2011.058941.

[6] W. J. Lammers, A. el-Kays, K. Arafat, and T. Y. el-Sharkawy, "Wave mapping: detection of co-existing multiple wavefronts in high-resolution electrical mapping," *Med. Biol. Eng. Comput.*, vol. 33, no. 3 Spec No, pp. 476–481, 1995, [Online]. Available: http://www.ncbi.nlm.nih.gov/pubmed/7666697.

[7] P. Du, G. O'Grady, J. U. Egbuji, W. J. Lammers, D. Budgett, P. Nielsen, J. A. Windsor, A. J. Pullan, and L. K. Cheng, "High-resolution mapping of in vivo gastrointestinal slow wave activity using flexible printed circuit board electrodes: methodology and validation," *Ann. Biomed. Eng.*, vol. 37, no. 4, pp. 839–846, 2009, doi: 10.1007/s10439-009-9654-9.

[8] G. O'Grady, T. H. H. Wang, P. Du, T. Angeli, W. J. Lammers, and L. K. Cheng, "Recent progress in gastric arrhythmia: Pathophysiology, clinical significance and future horizons," *Clin. Exp. Pharmacol. Physiol.*, vol. 41, no. 10, pp. 854–862, 2014, doi: 10.1111/1440-1681.12288.

[9] J. Y. H. Liu, P. Du, W. Y. Chan, and J. A. Rudd, "Use of a microelectrode array to record extracellular pacemaker potentials from the gastrointestinal tracts of the ICR mouse and house musk shrew (Suncus murinus).," *Cell Calcium*, vol. 80, pp. 175–188, Jun. 2019, doi: 10.1016/j.ceca.2019.05.002.

[10] J. Y. H. Liu, P. Du, and J. A. Rudd, "Acetylcholine exerts inhibitory and excitatory actions on mouse ileal pacemaker activity: role of muscarinic versus nicotinic receptors.," *Am. J. Physiol. Gastrointest. Liver Physiol.*, vol. 319, no. 1, pp. G97–G107, 2020, doi: 10.1152/ajpgi.00003.2020.

[11] R. Yassi, G. O'Grady, N. Paskaranandavadivel, P. Du, T. R. Angeli, A. J. Pullan, L. K. Cheng, and J. C. Erickson, "The gastrointestinal electrical mapping suite (GEMS): Software for analyzing and visualizing high-resolution (multi-electrode) recordings in spatiotemporal detail," *BMC Gastroenterol.*, vol. 12, 2012, doi: 10.1186/1471-230X-12-60.

[12] P. V Bayly, B. H. KenKnight, J. M. Rogers, R. E. Hillsley, R. E. Ideker, and W. M. Smith, "Estimation of conduction velocity vector fields from epicardial mapping data," *IEEE Trans. Biomed. Eng.*, vol. 45, no. 5, pp. 563–571, 1998, doi: 10.1109/10.641337.

[13] Z. Wang, A. C. Bovik, H. R. Sheikh, and E. P. Simoncelli, "Image quality assessment: from error visibility to structural similarity.," *IEEE Trans. Image Process.*, vol. 13, no. 4, pp. 600–12, Apr. 2004, doi: 10.1109/tip.2003.819861.

[14] J. D. Huizinga, J.-H. Chen, Y. F. Zhu, A. Pawelka, R. J. McGinn, B. L. Bardakjian, S. P. Parsons, W. A. Kunze, R. Y. Wu, P. Bercik, A. Khoshdel, S. Chen, S. Yin, Q. Zhang, Y. Yu, Q. Gao, K. Li, X. Hu, N. Zarate, *et al.*, "The origin of segmentation motor activity in the intestine.," *Nat. Commun.*, vol. 5, p. 3326, 2014, doi: 10.1038/ncomms4326.

[15] P. Du, N. Paskaranandavadivel, G. O'Grady, S. J. Tang, and L. K. Cheng, "A Theoretical Analysis of the Initiation, Maintenance and Termination of Gastric Slow Wave Re-entry," *J. Theor. Biol.*, vol. 2014, 2014.

[16] W. J. E. P. Lammers, "Spatial and temporal coupling between slow waves and pendular contractions.," *Am. J. Physiol. Gastrointest. Liver Physiol.*, vol. 289, no. 5, pp. G898-903, Nov. 2005, doi: 10.1152/ajpgi.00070.2005.

[17] P. Zhang, N. Aydemir, M. Alkaisi, D. E. Williams, and J. Travas-Sejdic, "Direct Writing and Characterization of Three-Dimensional Conducting Polymer PEDOT Arrays," *ACS Appl. Mater. Interfaces*, vol. 10, no. 14, pp. 11888–11895, Apr. 2018, doi: 10.1021/acsami.8b02289.